



## Combination of disulfiram and Copper–Cysteamine nanoparticles induces mitochondria damage and promotes apoptosis in endometrial cancer

Lijun Yang<sup>a,b,1</sup>, Cancan Yao<sup>a,b</sup>, Zhenning Su<sup>a,b</sup>, Yihao Fang<sup>c</sup>, Nil Kanatha Pandey<sup>d,e</sup>, Eric Amador<sup>d,e</sup>, Tian Diao<sup>a,b</sup>, Guo Bao<sup>b</sup>, Derong Cao<sup>c</sup>, Xihua Chen<sup>b</sup>, Xiangbo Xu<sup>b</sup>, Bin He<sup>b,\*\*</sup>, Yufeng Zheng<sup>a,f,\*\*\*</sup>, Wei Chen<sup>d,e,\*</sup>

<sup>a</sup> Chinese Academy of Medical Science and Peking Union Medical College, Beijing, 100730, China

<sup>b</sup> NHC Key Laboratory of Reproductive Health Engineering Technology Research, Department of Reproduction and Physiology, National Research Institute for Family Planning, Beijing 100081, China

<sup>c</sup> State Key Laboratory of Luminescent Materials and Devices, School of Chemistry and Chemical Engineering, South China University of Technology, Guangzhou, 510641, China

<sup>d</sup> School of CHIPS, Xian-Jiaotong Liverpool University, Suzhou 215123, China

<sup>e</sup> Department of Physics, University of Texas at Arlington, Arlington, TX, 76013, USA

<sup>f</sup> School of Materials Science and Engineering, Peking University, Beijing, 100871, China

### ARTICLE INFO

#### Keywords:

Combination

Disulfiram

Copper–Cysteamine nanoparticles

Mitochondria damage

Promotes apoptosis in Endometrial Cancer

### ABSTRACT

Endometrial cancer (EC) stands as one of the most prevalent gynecological malignancies affecting women, with its incidence and disease-related mortality steadily on the rise. Disulfiram (DSF), an FDA-approved medication primarily used for treating alcohol addiction, has exhibited promising anti-tumor properties. Studies have revealed DSF's capacity for enhanced anti-tumor activity, particularly when combined with copper. The novel Copper–Cysteamine (CuCy) compound,  $\text{Cu}_3\text{Cl}(\text{SR})_2$  ( $\text{R}=\text{CH}_2\text{CH}_2\text{NH}_2$ ), showcases photodynamic effects and demonstrates significant anti-tumor potential under various conditions, including exposure to ultraviolet light, X-ray, microwave, and ultrasound. This study delves into exploring the synergistic anti-tumor effects and underlying mechanisms by utilizing copper-cysteamine in conjunction with DSF against endometrial cancer. The investigation involved comprehensive analyses encompassing *in vitro* experiments utilizing Ishikawa cells, *in vivo* studies, and transcriptomic analyses. Remarkably, the combined administration of both compounds at a low dose of 0.5  $\mu\text{M}$  exhibited pronounced efficacy in impeding tumor growth, inhibiting blood vessel formation, and stimulating cell apoptosis. Notably, experiments involving transplanted tumors in nude mice vividly demonstrated the significant *in vivo* anti-tumor effects of this combination treatment. Detailed examination through transmission electron microscopy unveiled compelling evidence of mitochondrial damage, cellular swelling, and rupture, indicative of apoptotic changes in morphology due to the combined treatment. Moreover, transcriptomic analysis unveiled substantial downregulation of mitochondrial-related genes at the molecular level, coupled with a significant hindrance in the DNA repair pathway. These findings strongly suggest that the combined application of CuCy and DSF induces mitochondrial impairment in Ishikawa cells, thereby fostering apoptosis and ultimately yielding potent anti-tumor effects.

Peer review under responsibility of KeAi Communications Co., Ltd.

\* Corresponding author. Department of Physics, University of Texas at Arlington, Arlington, TX, 76013, USA.

\*\* Corresponding author.

\*\*\* Corresponding author. Graduate School of Peking Union Medical College, Beijing, 100730, China.

E-mail addresses: [284654233@qq.com](mailto:284654233@qq.com) (L. Yang), [iusuzy0511@163.com](mailto:iusuzy0511@163.com) (C. Yao), [2495296004@qq.com](mailto:2495296004@qq.com) (Z. Su), [974543621@qq.com](mailto:974543621@qq.com) (Y. Fang), [nil.pandey@mavs.uta.edu](mailto:nil.pandey@mavs.uta.edu) (N.K. Pandey), [eric.amador@mavs.uta.edu](mailto:eric.amador@mavs.uta.edu) (E. Amador), [2201111898@stu.pku.edu.cn](mailto:2201111898@stu.pku.edu.cn) (T. Diao), [baoguo\\_1985@126.com](mailto:baoguo_1985@126.com) (G. Bao), [drcao@scut.edu.cn](mailto:drcao@scut.edu.cn) (D. Cao), [xhchen.bio@outlook.com](mailto:xhchen.bio@outlook.com) (X. Chen), [xiangboxuhappy@126.com](mailto:xiangboxuhappy@126.com) (X. Xu), [hebin@nrifp.org.cn](mailto:hebin@nrifp.org.cn) (B. He), [yfzheng@pku.edu.cn](mailto:yfzheng@pku.edu.cn) (Y. Zheng), [Wei.Chen03@xjtu.edu.cn](mailto:Wei.Chen03@xjtu.edu.cn) (W. Chen).

<sup>1</sup> First author.

<https://doi.org/10.1016/j.bioactmat.2024.02.009>

Received 18 December 2023; Received in revised form 25 January 2024; Accepted 7 February 2024

2452-199X/© 2024 The Authors. Publishing services by Elsevier B.V. on behalf of KeAi Communications Co. Ltd. This is an open access article under the CC BY-NC-ND license (<http://creativecommons.org/licenses/by-nc-nd/4.0/>).

## 1. Introduction

Endometrial cancer (EC), situated in the epithelial lining of the endometrium [1], stands as one of the most prevalent gynecological malignancies in women, with its global incidence and disease-related mortality showing a steady increase [2–4]. Despite advancements, challenges persist, such as tumor recurrence, radiation-induced damage to normal tissues, varying individual responses to drugs, and the emergence of tumor resistance to existing medications. Enhancing the life expectancy of patients remains an ongoing formidable challenge.

The development of novel drugs is both expensive and prone to a high failure rate, involving prolonged testing periods. Utilizing already approved drugs for diverse diseases as potential anti-tumor therapeutics presents a faster, cost-effective alternative. These drugs have exhibited patient tolerance and possess clinically applicable formulations [5].

Disulfiram (DSF), an FDA-approved medication primarily used to treat alcohol addiction [6], has undergone rigorous evaluation regarding its pharmacokinetics, safety, and tolerability [7]. Multiple studies suggest its potential as an anti-tumor agent [8–11]. In specific cases like inflammatory breast cancer and gliomas, combining DSF with copper has demonstrated remarkable antitumor activity [12,13]. DSF undergoes metabolic processes within the human body, forming diethyldithiocarbamate (DTC), which complexes with  $\text{Cu}^{2+}$ , resulting in DTC-copper complex (bis (diethyldithiocarbamate)-copper (CuET)) accumulation in tumors. Within cells, CuET interacts with NPL4, an

adaptor of p97 (also known as Valosin-containing protein, VCP) segregase, causing aggregation and subsequent failure of the p97-NPL4-UFD1 pathway, leading to cell death [5]. UFD1 is Ubiquitin recognition factor in ER-associated degradation protein 1. DSF and elesclomol (ES) are both Copper ionophores [12,14], and they help copper get into cells or organelles. Overloading of copper ions in mitochondria with the help of copper ionophore ES causes aggregation of lipoylated proteins and reduction of Fe-S proteins, triggering proteotoxicity and ultimately cell death [15]. Findings on Copper-Copper ionophore-induced cell death suggest that Copper-Copper ionophores may be a potential therapeutic tool for cancer.

Cysteamine ( $\text{HSCH}_2\text{CH}_2\text{NH}_2$ ) is a small organic molecule with active thiol and amino groups, involved in various physiological functions within the human body and utilized in the treatment of several diseases [16,17]. Its robust metal affinity enables chemical reactions with numerous transition metals [18]. Copper (Cu) serves as an essential trace nutrient vital for various physiological processes across cell types, acting as a critical catalytic co-factor in diverse biological processes. Hence, Copper-Cysteamine (CuCy) complexes serve as suitable model compounds, enhancing the fundamental understanding of copper-containing enzymes [19]. The novel CuCy complex,  $\text{Cu}_3\text{Cl}(\text{SR})_2$  ( $\text{R}=\text{CH}_2\text{CH}_2\text{NH}_2$ ), exhibits photodynamic effects, generating singlet oxygen under light or X-ray activation [20], displaying anti-tumor effects under various conditions including ultraviolet light, X-ray, microwave, or ultrasound [21–29]. When combined with DSF, it significantly

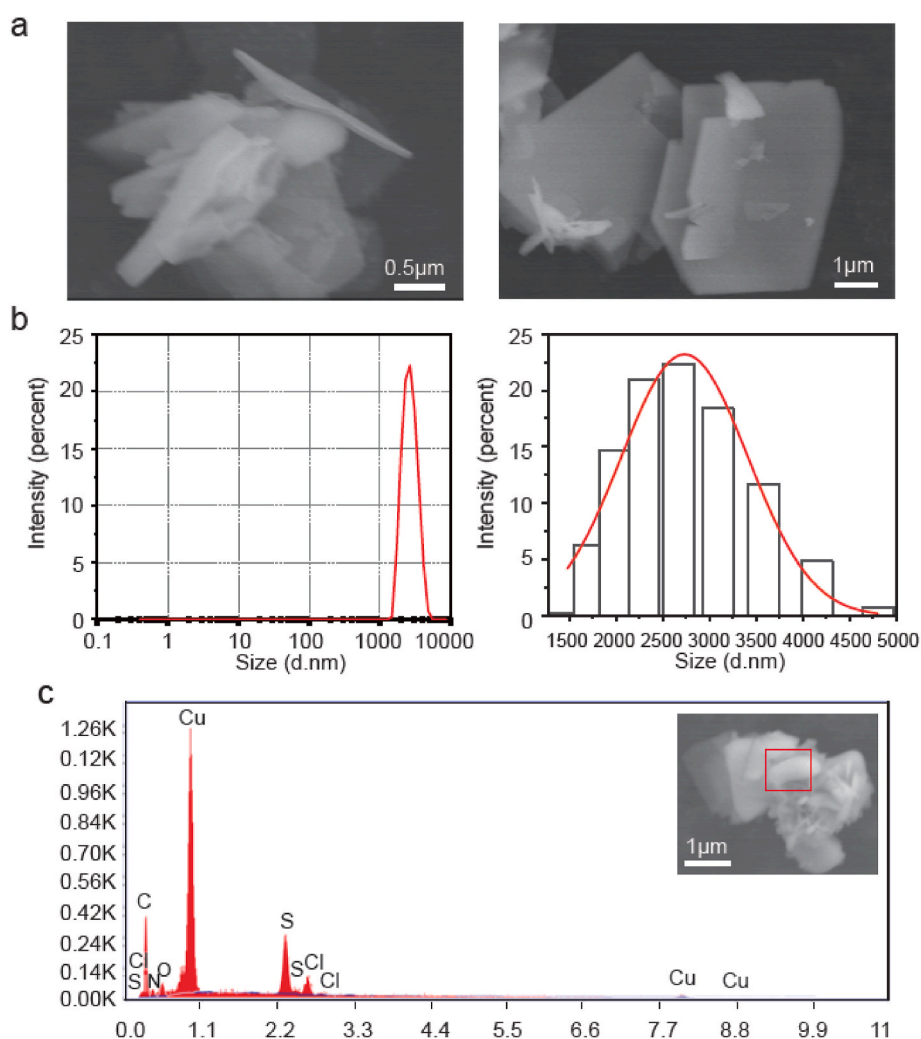


**Fig. 1.** Material characterization. (a) Scanning Electron Microscopy (SEM) image and (b) Particle size of CuCy; (c) Energy Dispersive Spectroscopy (EDS) analysis of CuCy.

augments anti-tumor effects, as observed in esophageal cancer [30].

This study rigorously examined the combined effects of CuCy and DSF on endometrial cancer cells (Ishikawa). Determination of optimal concentrations for the combined treatment was achieved through extensive *in vitro* experiments. The investigation delved into elucidating the mechanisms of material entry into cells and subsequent alterations in cellular phenotype during the combined treatment. Validating the anti-tumor efficacy of the combined treatment was accomplished *in vivo* using nude mice. Transcriptome sequencing was employed to delve into the molecular mechanisms underpinning the anti-tumor effects of these drugs.

## 2. Materials and methods

### 2.1. Materials

CuCy nanoparticles were synthesized as previous publications [20]. Briefly described below: Copper (II) chloride dihydrate (99.99%), 2-mercaptoethylamine hydrochloride (cysteamine hydrochloride or Cys, 98%) and sodium hydroxide (98%) were purchased from Sigma (USA).  $\text{CuCl}_2 \cdot 2\text{H}_2\text{O}$  (0.460 g, 2.698 mmol) was dissolved in DI water followed by addition of cysteamine (0.636 g, 8.244 mmol). The pH of the solution was adjusted to 8 using 2.5 M NaOH and stirred for 2 h at room temperature. The solution is then heated to boiling for 30 min. Crystals of  $\text{Cu}_3\text{Cl}(\text{SR})_2$  were precipitated from the solution and the supernatant was discarded. The obtained  $\text{Cu}_3\text{Cl}(\text{SR})_2$  crystals were further centrifuged and washed using a mixture of DI water and ethanol (v/v = 5 : 4) three times. Finally, the crystals were dried completely in a vacuum oven at room temperature overnight.

#### 2.1.1. Material characterizations and elemental analysis

The surface characteristics of CuCy powder were observed under a scanning electron microscope (SEM, S-4800, Hitachi) and its elemental composition was studied with the equipped Energy-Disperse X-ray Spectroscopy (EDS). The material CuCy was dispersed in DI water, sonicated for 1 h, mixed and analyzed by Dynamic light scattering (DLS, Zetasizer Nano ZS90, Malvern).

### 2.2. *In vitro* study

#### 2.2.1. Cell culture

Ishikawa cells and human umbilical vein endothelial cells (HUVECs) were purchased from the National Experimental Cell Resource Sharing Platform. Ishikawa cells were cultured in Dulbecco's Modified Eagle medium with 4.5 g/l Glucose (DMEM, Gibco, USA), supplemented with 10% fetal bovine serum (FBS, Gibco, Australia), 100 U/mL penicillin, and 100 µg/mL streptomycin (Gibco, USA). HUVEC cells were cultured in Endothelial Cell Medium (ECM, ScienCell, USA), supplemented with 10% fetal bovine serum, 100 U/mL penicillin, 100 µg/mL streptomycin and 1% Endothelial Cell Growth Supplement. The cells were cultured in a humidified atmosphere at 37 °C with 5%  $\text{CO}_2$ . The second generation of cells after revival was used for experiments.

#### 2.2.2. Cytotoxicity test

Ishikawa cells were utilized to investigate the anti-tumor effects of CuCy and DSF (HY-B0240, MedChemExpress). CuCy was dispersed with DI water at 1 mg/mL, sonicated for 1 h, vortexed and mixed to obtain 2635 µM CuCy. Dimethyl sulfoxide (DMSO) was used to dissolve the DSF to get 100,000 µM DSF. Further dilution was done with the medium to get the concentration we needed. The Ishikawa cells were seeded in a 96-well plate and cultured in a 37 °C constant temperature incubator for 24 h. The negative control group received complete culture medium without any drugs, the blank control group contained only complete culture medium without cells, and the experimental group was treated with culture medium containing different concentrations of drugs. Each well received 200 µL, with 5 replicates per group, and the treatment

lasted for 24 h. At the end of the experiment, the supernatant was discarded, and fresh culture medium with 10% CCK-8 (Dojindo Molecular Technologies, Japan) was added. The reaction took place in a 37 °C incubator for 2–3 h, and absorbance of each well were detected at 450 nm by a microplate reader (Synergy 2, BioTek).

#### 2.2.3. Live/dead cell staining

Ishikawa cells were seeded in 6-well plates and cultured in a 37 °C incubator for 24 h. The original culture medium was removed, and different drug treatments were administered for each group (NC group: complete culture medium; CuCy group: 0.5 µM CuCy; DSF group: 0.5 µM DSF; CuCy + DSF group: 0.5 µM CuCy + 0.5 µM DSF). Every well received 2 mL of culture medium for 24 h, 3 replicate every group. At the end of the experiment, following the kit manual (C0021, Pulilai), staining working solution (working concentration of 2 µM for Calcein-AM and 5 µM for PI) was prepared. The cells were harvested after digestion and centrifugation (1000 rpm, 3 min). The supernatant was discarded, and the cells were washed three times with 1xPBS buffer (pH 7.4) to remove residual esterase activity. A cell suspension was prepared to achieve a density of  $5 \times 10^5$  cells/mL. Then, 100 µL of the staining working solution was added to 200 µL of the cell suspension, thoroughly mixed, and incubated at 37 °C for 15 min. Fluorescence was observed and images were captured under a fluorescence microscope.

#### 2.2.4. Angiogenesis assay

HUVEC cells were used for *in vitro* studies on the impact of CuCy and DSF on angiogenesis. Matrigel (356,234, Corning) was mixed with serum-free ECM culture medium in a 1:1 ratio, and 50 µl per well was evenly added to a 96-well plate, avoiding bubble formation. The plate was placed in a 37 °C incubator for 60 min to allow the gel to solidify. HUVEC cells cultured in a T25 flask until reaching approximately 80% confluency were collected. Following two washes with 1xPBS, the cells were resuspended in 1xPBS and divided into four equal parts. After centrifugation, the cells were collected and resuspended in different culture media (NC group: serum-free ECM culture medium; CuCy group: serum-free ECM culture medium containing 0.5 µM CuCy; DSF group: serum-free ECM culture medium containing 0.5 µM DSF; CuCy + DSF group: serum-free ECM culture medium containing 0.5 µM CuCy and 0.5 µM DSF). The cell density was adjusted to  $2.5 \times 10^4$  cells/100 µL for every group. Then, 100 µL of HUVEC cells suspension was added to the above 96-well plate every well, 3 replicates per group. The plate was placed in a 37 °C incubator, and angiogenesis was observed under a microscope at hourly intervals. Photographs were taken when blood vessels were clearly formed in the control group.

#### 2.2.5. Apoptosis assay

Ishikawa cells were seeded in 6-well plates and treated as previously described for 24 h. After that, the cells were harvested and managed as the manufacturer's protocol (AD10, Dojindo). Briefly, the cells were washed twice with cold PBS, and the cell pellet was collected into flow tubes. Annexin V-APC and PI solution were added into the tube and mixed gently, and then the cells were incubated at room temperature for 15 min in the dark, followed by adding 400 µL  $1 \times$  Binding Buffer to each tube, mixed and analyzed by flow cytometry.

#### 2.2.6. Colony formation assay

Ishikawa cells were collected and seeded into 6-well plates with 5000 cells per well, and cultured at 37 °C for 24 h. The cells were treated as follows: (NC group: complete medium; CuCy group: 0.5 µM CuCy; DSF group: 0.5 µM DSF; CuCy + DSF group: 0.5 µM CuCy + 0.5 µM DSF, 3 replicates per group), and continue to culture for about 10 days until clonal clusters were formed. When the experiment was terminated, the cells were washed with 1xPBS for 3 times, fixed with 4% paraformaldehyde for about 15 min, stained with 0.5% crystal violet staining solution for 15 min, followed by rinsing with deionized water and air-drying before capturing images.

### 2.2.7. Mitochondrial membrane potential assay

Ishikawa cells were seeded in 6-well plates and cultured at 37 °C for 24 h, cells were treated with drugs for 12 h (NC group: complete culture medium; CuCy group: 0.5 μM CuCy; DSF group: 0.5 μM DSF; CuCy + DSF group: 0.5 μM CuCy + 0.5 μM DSF). Each group had three replicate wells, and each well contained 2 mL of culture medium. After discarding the culture medium, cells were washed once with PBS, followed by the addition of 1 mL of cell culture medium and 1 mL of JC-1 staining working solution (M8650, Solarbio). The mixture was thoroughly mixed and incubated at 37 °C in a cell culture incubator for 20 min. After the incubation period, the supernatant was removed, and cells were washed twice with JC-1 staining buffer (1x). Subsequently, 2 mL of cell culture medium was added, and the fluorescence was observed under a fluorescence microscope.

### 2.2.8. Observation of apoptosis through DAPI staining

Cells were inoculated into 6-well plates, adhered for 24 h. After 12 h of treatment (same treatment as before), discard the culture medium. Wash the cells once with 1x PBS. Discard the wash solution and fix the cells with 4% paraformaldehyde for 15 min. Wash the cells once with 1x PBS. Perforated with 1 mL of 0.1% Triton X-100 for 10 min. Washed twice with 1xPBS, and the results were observed under a fluorescence microscope.

### 2.2.9. Western blotting

After 12 or 24 h of drug treatments (same treatment as before), cells were harvested. Total protein was extracted and the protein concentration was determined by BCA method. 10% SDS-PAGE polyacrylamide gels were prepared, and protein samples (25 μg per well) were mixed with 5x loading buffer, and denatured in a 95 °C metal bath for 15 min. The denatured samples were loaded into the wells, and electrophoresis was performed at a constant voltage of 90 V. The protein bands were transferred onto PVDF membrane at a constant current of 300 mA for 1 h. The PVDF membranes were blocked with 10% skimmed milk at room temperature for approximately 3 h. After blocking, the PVDF membrane was incubated overnight at 4 °C with primary antibodies anti-Caspase-9 (A18676, Abclonal, diluted at 1:1000), anti-Caspase-3 (A19654, Abclonal, diluted at 1:1000) and anti-β-actin (AC038, Abclonal, diluted at 1:50,000). Anti-caspase-9 can recognize both pro-caspase-9 and cleaved-caspase-9, anti-caspase-3 can recognize both pro-caspase-3 and cleaved-caspase-3. The PVDF membrane was washed three times with 1x TBST for 5 min every time. The corresponding secondary antibodies were diluted in antibody dilution buffer and incubated at room temperature for 1 h. The PVDF membrane was washed three times with 1x TBST for 5 min every time, chemiluminescent substrate was prepared, and images were captured using LAS 4000.

### 2.2.10. Transmission electron microscopy (TEM) observations

Ishikawa cells were cultured in T25 culture flasks until reaching approximately 80% cell density. The experimental group (CuCy + DSF group) was treated with 0.5 μM CuCy and 0.5 μM DSF for 20 h, while the control group (NC group) was cultured with complete medium without any drugs, The CuCy-500 group was treated with 500 μM CuCy for 3 h. After removing the culture medium, the cells were fixed with electron microscope fixative (G1102, Servicebio) at 4 °C for 4 h, carefully collect the cells using a cell scraper. Cells were collected by centrifugation and washed 3 times with 1x PBS for 3 min each time. The cell precipitate obtained by centrifugation was wrapped in the 1% agarose and fixed with 1% OsO<sub>4</sub> (18,456, Ted Pella Inc) in 0.1 M PBS (pH 7.4) in the dark for 2 h at room temperature. After remove OsO<sub>4</sub>, the samples were rinsed in 0.1 M PBS (pH 7.4) for three times, 15 min each and dehydrated in a gradient of ethanol (30%, 50%, 70%, 80%, 95%, 100% I, 100% II) for 20 min each and 100% acetone twice for 15 min each. The samples undergo the following steps for penetration embedding: Acetone:EMBed 812 (90,529-77-4, SPI) = 1:1 for 2–4 h at 37 °C; Acetone:EMBed 812 = 1:2 overnight at 37 °C; pure EMBED 812 for 5–8 h

at 37 °C; Pour the pure EMBED 812 into the embedding models and insert the samples into the pure EMBED 812, and then overnight at 37 °C. The samples were moved into 65 °C oven to polymerize for more than 48h. The resin blocks were cut to 60–80 nm thick slices by the ultramicrotome (Leica UC7, Leica), and fished out onto the 150 meshes cuprum grids with formvar film. Copper grids were stained in a solution saturated with 2% uranyl acetate in ethanol for 8 min in the dark, washed three times with 70% ethanol, rinsed three times with ultrapure water, stained with 2.6% lead citrate solution avoiding carbon dioxide for 8 min, washed three times with ultrapure water, and gently dried on filter paper. The copper grids were placed in copper grid boxes and air-dried overnight at room temperature. Observation and image collection analysis were performed using transmission electron microscopy (HT7800, Hitachi).

### 2.2.11. Transcriptome sequencing analysis

Ishikawa cells were seeded into a 6-well plate. After 24 h, the experimental group (CuCy + DSF group) was treated with 0.5 μM CuCy and 0.5 μM DSF for 12 h. The control group (NC group) was cultured with complete medium without any drugs, 3 replicates per group. Total RNA was extracted using the Trizol reagent (Invitrogen, CA, USA) according to the manufacturer's protocol. RNA integrity was assessed using the Agilent 2100 Bioanalyzer (Agilent Technologies, Santa Clara, CA, USA). Then the libraries were constructed using VAHTS Universal V6 RNA-seq Library Prep Kit according to the manufacturer's instructions. The libraries were sequenced on an Illumina NovaSeq 6000 platform and 150 bp paired-end reads were generated. Raw reads of fastq format were firstly processed using fastp [31] and the low quality reads were removed to obtain the clean reads. Then the clean reads were mapped to the reference genome using HISAT2 [32]. FPKM [33] of each gene was calculated and the read counts of each gene were obtained by HTSeq-count [34]. PCA analysis was performed using R (v 3.2.0) to evaluate the biological duplication of samples. Differential expression analysis was performed using the DESeq2 [35]. Q value < 0.05 and foldchange >2 or foldchange <0.5 was set as the threshold for significantly differential expression gene (DEGs). Based on the hypergeometric distribution, GO enrichment analysis [36] of DEGs were performed to screen the significant enriched term using R (v 3.2.0). Gene Set Enrichment Analysis (GSEA) was performed using GSEA software [37, 38].

## 2.3. In-vivo animal study

### 2.3.1. Animals

The antitumor effects of the two drugs were examined in an endometrial cancer xenograft model using Female BALB/c nude mice (5–6 weeks, weighing 16–18g) purchased from Beijing Vital River Laboratory Animal Technology Co. Ltd (Beijing, China). They were housed according to standard care protocols, and all nude mice were acclimatized to the environment for one week before experiments were carried out. All protocols for animal care and treatment were approved by the Ethical Committee of National Research Institute for Family Planning.

### 2.3.2. Tumor xenograft model and tumor administration in nude mice

For the tumor xenografts, 3 × 10<sup>6</sup> cells/100 μL Ishikawa cells were inoculated on the backs of nude mice. Tumor volumes were observed daily, the length (L, mm) and width (W, mm) of the transplanted tumor were measured using caliper. Tumor volume was calculated using the formula:  $V = 0.52 \times L \times W^2$  [39]. When the average tumor volume reached about 50 mm<sup>3</sup> [40], the nude mice were random divided into for group. The control group (NC) received 30 μL of saline; the CuCy group 30 μL 0.5 μM CuCy; the DSF group 30 μL 0.5 μM DSF solution; and the CuCy + DSF group 30 μL both CuCy (0.5 μM) and DSF (0.5 μM) by local injection into tumor tissues every 3 days. mice weight and tumors size were recorded. After 5 times drug administration or the average tumor size in the controls reached 1000mm<sup>3</sup>, which met the criterion for euthanasia.

blood samples, tumors and major organs of mice were collected. Subsequently, and major organs were fixed in 4% paraformaldehyde (Sigma- Aldrich, USA) for further analysis.

### 2.3.3. Blood biochemical analysis

Serum was obtained by centrifuged (3000 rpm, 10 min). The levels of alanine transaminase (ALT), aspartate transaminase (AST), gamma-glutamyl transferase ( $\gamma$ -GT), urea (UREA), creatinine (CREA), and uric acid (UA) in the serum were analyzed by Wuhan Servicebio Technology Co., Ltd.

### 2.3.4. H&E

The embedding and staining process follows a similar procedure as described in the literature [41,42]. Fixed tumors and visceral tissues were dehydrated by graded alcohol (70%, 75%, 80%, 95% I and II, and 100% I and II) for 15 min each, followed by xylene I and II for 15 min each, paraffin I and II for 1 h, and then paraffin embedded. After embedding, the tissues were sectioned into 5- $\mu$ m-thick slices and affixed to adhesive slides, which were baked at 65 °C for 1.5 h, dewaxed in xylene I and II for 15 min each, then hydrated in a gradient of ethanol (100% I and II, 95% I and II, 85%, 75%) for 5 min each, followed by a 5-min treatment with deionized water, and then stained with Hematoxylin and Eosin (H&E), and then sealed with a resin after final graded-alcohol dehydration. staining results were observed by light microscopy and images were captured.

### 2.3.5. TUNEL method

Tumor tissues embedded in paraffin were sectioned into 5  $\mu$ m-thick slices and affixed to adhesive glass slides. The slides were baked at 65 °C for 1.5 h, dewaxed in xylene I and II for 15 min each, and hydrated in a gradient of ethanol (100% I and II, 95% I and II, 85%, 75%) for 5 min each, followed by a 5-min treatment with deionized water. Proteinase K (20  $\mu$ g/mL) without DNase was added, and the reaction was carried out at 37 °C for 30 min. The samples were washed three times with 1x PBS. The TUNEL detection solution was prepared following the kit instructions (C1088, Biyuntian), with a TdT enzyme to fluorescent labeling ratio of 1:9. Fifty microliters of the TUNEL detection solution were added to the samples and incubated at 37 °C in the dark for 60 min. After washing three times with 1x PBS, the samples were observed under a fluorescence microscope.

## 2.4. Statistical analysis

In this study, the data are shown as the mean values  $\pm$  standard deviation. The statistical difference was analyzed using the unpaired *t*-test and defined it as significant differences when  $p < 0.05$ .

## 3. Results

### 3.1. Characterization of materials

When observed under scanning electron microscopy (SEM), CuCy particles manifest an irregular flake-like structure (Fig. 1a). The DLS results show that the size of CuCy is normally distributed, Z-Average size is 2463 nm, Peak size is 2701 nm (Fig. 1b), which is consistent with the SEM results. Elemental analysis conducted through Energy Dispersive Spectroscopy (EDS) identified the presence of S, C, N, Cl, and O elements (Fig. 1c). It's noteworthy that the molecular formula of CuCy, is  $\text{Cu}_3\text{Cl}(\text{SR})_2$  (where  $\text{R}=\text{CH}_2\text{CH}_2\text{NH}_2$ ), and the detected O element might originate from oxygen in the surrounding air.

### 3.2. Anti-tumor efficacy assessment

A comparative assessment of cytotoxicity between  $\text{CuCl}_2$  and CuCy was conducted since CuCy is synthesized from  $\text{CuCl}_2$ . The evaluation on Ishikawa cells revealed that at concentrations around 100  $\mu\text{M}$ , CuCy

exhibited notably higher cytotoxicity compared to  $\text{CuCl}_2$ , resulting in a cell survival rate below 50% (Fig. 2a). Further investigation compared the cytotoxic effects of  $\text{CuCl}_2$ , CuCy, and DSF individually on tumor cells within a drug concentration range of 12.5–200  $\mu\text{M}$ . DSF demonstrated the most potent anti-tumor effect at concentrations of 50  $\mu\text{M}$  or higher, followed by CuCy, while  $\text{CuCl}_2$  exhibited the weakest effect (Fig. 2b). The study also evaluated various concentrations of combined therapy using CuCy and DSF to ascertain their anti-tumor effects (Fig. 2c). Remarkably, at concentrations of both drugs set at 0.5  $\mu\text{M}$ , significant tumor cell eradication was achieved at this low dosage. Consequently, the 0.5  $\mu\text{M}$  combined therapy was selected for subsequent studies. An experiment employing cell viability/death staining revealed that compared to both the control group and individual drug use at 0.5  $\mu\text{M}$ , the combination therapy significantly augmented the cytotoxic effect on tumor cells (Fig. 2d).

An important finding was that the combination of CuCy and DSF allowed for a substantial reduction in drug dosages. This reduction is of significant importance as it minimizes the likelihood of inducing adverse reactions within the body.

### 3.3. Phenotypic studies

The acquisition of sustained angiogenesis capability is a critical hallmark feature in the initiation and progression of cancer [43–45]. Similar to normal tissues, tumors rely on nutrients and oxygen while eliminating metabolic waste and carbon dioxide. This demand is met by the tumor-associated neovascular system. Initially, cells in early-stage abnormal proliferative lesions lack angiogenic abilities, constraining their expansion. However, for early-stage tumors to grow larger, they must acquire angiogenesis capability [46,47]. As tumors reach a certain size, they start invading surrounding tissues, including blood vessels and lymphatic vessels. This vascular invasion allows shed tumor cells to circulate through the bloodstream, seeding new locations and forming metastatic foci (Fig. 3a). Consequently, blood vessels play a pivotal role in tumor growth and development.

In studying the effects of drugs on angiogenesis, HUVEC cells were utilized. Notably, the combination drug group significantly inhibited angiogenesis by the 3rd hour, and by the 5th hour, even the few nodes that had formed were disrupted. This suggests that the drug combination not only affects angiogenesis but also dismantles already formed blood vessels. Conversely, there was no significant difference observed between the single-drug groups and the control group (Fig. 3b). Comparison between the control group and both the combination drug group and the DSF group indicated a noteworthy increase in the rate of cell apoptosis, signifying a substantial promotion of cell apoptosis. However, the CuCy single-drug group didn't display a significant deviation from the control group (Fig. 3c and d). In the clonogenic formation assay results (Fig. 3e), the combination drug group barely formed cell colonies, whereas the DSF group exhibited scattered few colonies. Both groups showed a significant reduction in the number of colonies compared to the control group. In contrast, the CuCy group didn't significantly differ in the number of cell colonies formed compared to the control group. This suggests that both long-term DSF use and the combination drug group can notably diminish the survival and growth capability of tumor cells.

### 3.4. In vivo study

To investigate tumor responses to drugs *in vivo*, BALB/c nude mice were employed for the experiments. Each mouse was inoculated with 3 million Ishikawa cells, and drug administration commenced when the tumor size reached approximately 50  $\text{mm}^3$  (Fig. 4a). Notably, the tumors in the NC group exhibited significantly larger size and weight compared to the other groups (Fig. 4b and c). The growth curve of transplanted tumors during drug administration revealed a considerably higher tumor growth rate in the NC group compared to others. Conversely,

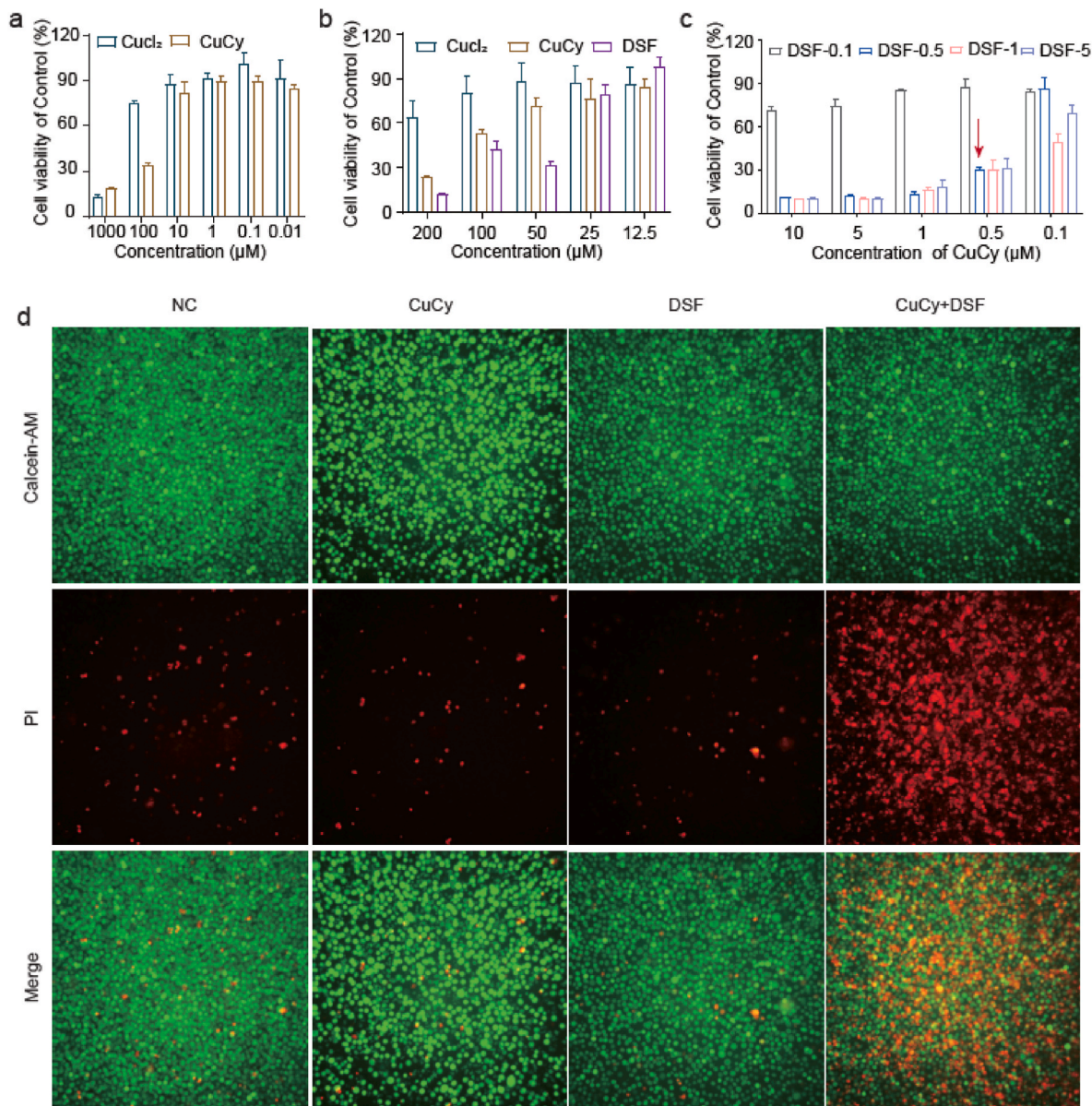


**Fig. 2.** *In vitro* antitumor effect studies of drugs. (a) Cytotoxic effects of different concentrations of CuCl<sub>2</sub> and CuCy, (b) different concentrations CuCl<sub>2</sub>, CuCy, and DSF and (c) Combination therapy with different concentrations of CuCy and DSF on Ishikawa cells; (d) Cell live/dead staining assay when CuCy and DSF were used alone at 0.5 μM or in combination at 0.5 μM.

tumor growth was notably inhibited in the CuCy and CuCy + DSF groups. In the DSF group, tumors exhibited a gradual decrease in size from the 6th day onwards, indicating a significant anti-tumor effect of DSF *in vivo* (Fig. 4d). Over the duration of tumor burden, all groups of mice experienced weight loss, with the DSF single-drug group displaying the fastest decline and the combination drug group demonstrating the slowest decline (Fig. 4e).

ALT, AST, and  $\gamma$ -GT are three indicators commonly used to reflect liver function [48], while CREA, UA, and BUN reflect kidney function [49]. Biochemical analysis of serum indicators reflecting liver and kidney function was performed. ALT, AST, and  $\gamma$ -GT indicated normal liver function across all groups (Fig. 4f–h). BUN levels were within the normal range for all groups (Fig. 4i). UA levels in the NC group were normal, while in the other groups, variations between normal and below-normal levels were observed. However, the proportion below the normal range was higher in the DSF-only group compared to the CuCy-containing group (Fig. 4j). Concerning the CREA indicator, the NC and CuCy groups were within the normal range, while the DSF and CuCy + DSF

groups exhibited values slightly below the lower limit of the normal range (Fig. 4k). H&E staining of major organs did not reveal any noticeable abnormalities across the four groups of mice (Fig. 4l). Additionally, H&E staining of tumor tissues showed regional tumor cell death in all three drug-treated groups, further confirmed by subsequent TUNEL staining, indicating apoptosis. Notably, the DSF and combination drug groups exhibited a significantly higher number of apoptotic cells compared to the control group. The TUNEL method [50], widely used for detecting cell apoptosis in histological research, confirmed these findings [51].

The *in vivo* experiments demonstrated that DSF, administered alone at 0.5 μM or in combination with CuCy, significantly inhibited tumor growth. However, the DSF single-drug group experienced more pronounced weight loss compared to the combination drug group, potentially impacting mouse kidney function. This suggests that when DSF is administered alone, its side effects on the mouse body are more pronounced. Conversely, in the presence of CuCy, DSF might be more localized to the transplanted tumor area, reducing its impact on other

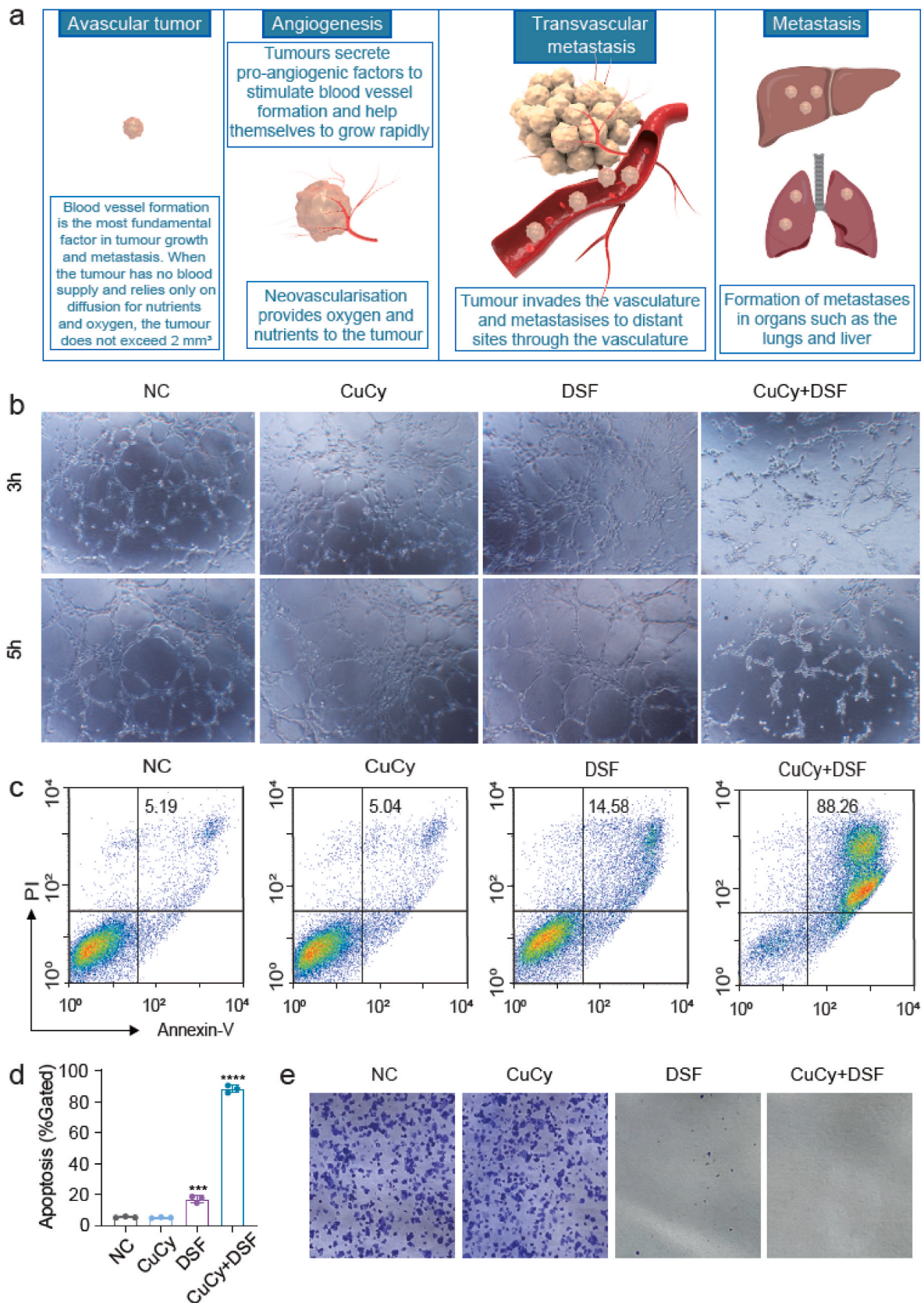


**Fig. 3.** Phenotyping experimental studies. (a) Schematic diagram of the role of vessels in the process of tumor growth and metastasis; (b) Vessel formation assay of HUVEC cells after drug treatment; (c) Detection of apoptosis by flow cytometry after 24 h of drug treatment and (d) histogram of the number of apoptotic cells among groups; (e) clone formation assay. \*\*\*\* $P \leq 0.0001$ , \*\*\* $P \leq 0.001$  when different groups compared with the NC group.

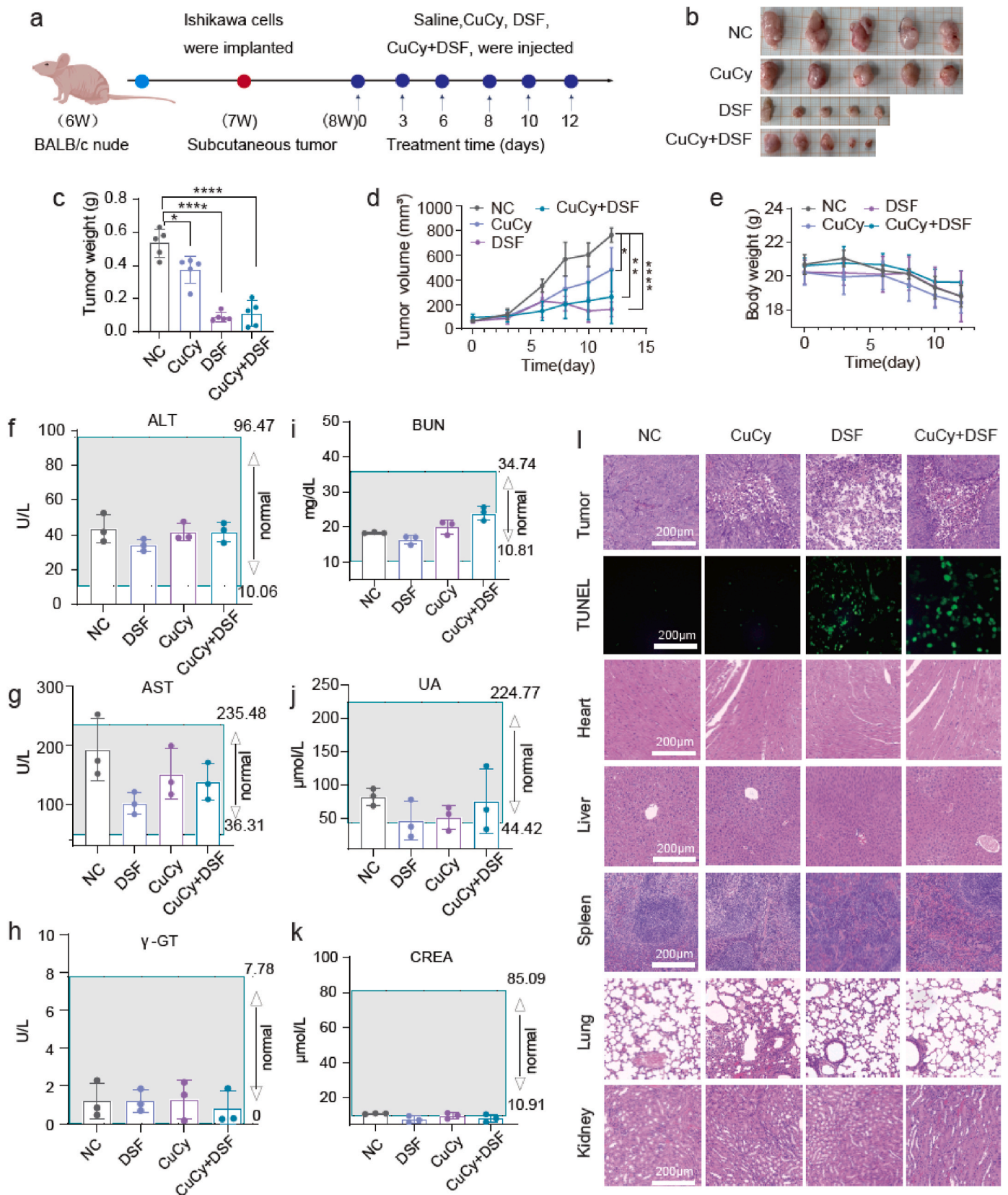


**Fig. 4.** *In vivo* experiments to study the anti-tumor effect of CuCy and DSF. (a) Schematic diagram of subcutaneous transplanted tumors and drug administration in nude mice; (b) Size and (c) Weight of the transplanted tumors ( $n = 5$ ); (d) Growth curve of the transplanted tumors *in vivo* ( $n = 5$ ); (e) Mouse body weight changes during drug treatment ( $n = 5$ ); (f–h) Serum levels of ALT, AST,  $\gamma$ -GT, indicators of hepatic function, and (i–k) CREA, UA, and BUN, indicators of renal function, in the mouse ( $n = 3$ ); (l) Results of H&E staining for subcutaneously transplanted tumors and organs (heart, liver, spleen, lung, kidney) in mice. Additionally, TUNEL staining results for the transplanted tumors. Data are represented as the mean  $\pm$  SD. \*\*\*\* $P \leq 0.0001$ , \*\* $P \leq 0.01$  and \* $P \leq 0.05$  when different groups compared with the NC group.

parts of the body and alleviating DSF-induced side effects. Thus, the combination of DSF and CuCy not only markedly inhibits tumor growth but also mitigates side effects *in vivo*.

### 3.5. TEM observations

A macroscopic examination was conducted to explore material entry pathways and cellular responses. Normal Ishikawa cells, viewed under low magnification, exhibited an elliptical appearance with uniform cytoplasm. The cell nucleus (N), also elliptical, displayed prevalent euchromatin dominance. A distinct nucleolus (Nu) with sparse structure was observed, while the nuclear membrane appeared clear (Fig. 5a, left). Under higher magnification, mitochondria (M) exhibited mostly intact structures with clear membranes, uniform matrices, visible cristae, and the rough endoplasmic reticulum (RER) showed minimal expansion with no noticeable ribosome surface disaggregation (Fig. 5a, right).

In the experimental group treated with a combination of CuCy (0.5  $\mu\text{M}$ ) and DSF (0.5  $\mu\text{M}$ ) for 20 h, cells displayed an elliptical shape trending towards apoptosis, maintaining intact cell membranes and denser cytoplasm. The cell nucleus (N) exhibited irregular shapes, local invaginations, chromatin condensation, and partial fuzziness of the nuclear membrane (Fig. 5b1, upper). Mitochondria (M) displayed uneven sizes, intact membranes, sparse matrix, fractured cristae, and the RER exhibited slight expansion with the presence of autophagic vacuoles (AP) (Fig. 5b1, lower). Severe vacuolization suggestive of apoptosis was prominent (Fig. 5b2,3, upper). Organelles were extensively damaged, with the presence of autophagic vacuoles (Fig. 5b2, lower). Mitochondria exhibited swelling, membrane rupture, matrix lightning, dissolution, and reduced cristae (Fig. 5b3, lower). Although all cells in the experimental group were in an apoptotic state, no discernible CuCy particles were observed within the cells. Speculatively, the low concentration of CuCy might pose challenges in capturing the material trace inside the cells.

To elucidate the material entry pathway, the study increased the material concentration (500  $\mu\text{M}$ ) and reduced treatment time (3h). TEM observations revealed material edge morphology consistent with SEM findings (Fig. 1a). The material appeared in contact with the cell membrane, inducing local invagination (Fig. 5c1, top image). Upon material entry, a distinct lamellar membrane surrounded it, and autophagolysosomes (ASS) were observed around the material (Fig. 5c3, upper and lower). In the CuCy-500 $\mu\text{M}$  group, dispersed particles within the cytoplasm, encircled by membranes, suggested material entry through phagocytosis.

### 3.6. Transcriptomic analysis

Transcriptomic analysis was employed to explore the cytotoxic mechanisms behind combined drug therapy on Ishikawa cells. The control group received no treatment, while the experimental group was exposed to a combination of CuCy (0.5  $\mu\text{M}$ ) and DSF (0.5  $\mu\text{M}$ ) for 12 h, after which RNA was collected for sequencing analysis. Differentially expressed genes (DEGs) were identified as those exhibiting expression differences greater than 2-fold and a p-value less than 0.05 between the control and treatment groups.

Principal Component Analysis (PCA) highlighted significant distinctions between the control and drug-treated groups, revealing good biological replicability within each group (Fig. 6a). Within the combination therapy group, 5620 genes were upregulated, while 2251 genes were downregulated in comparison to the control group (Fig. 6b). The cluster heatmap (Fig. 6c) visually represented genes with relatively higher expression in orange and red, and those with lower expression in blue. The volcano plot (Fig. 6d) depicted the overall distribution of DEGs. Gene Ontology (GO) enrichment analysis (Fig. 6e, detailed in Table S1) described the functions of these DEGs. The Circular plot highlighted GO:0005509 with the smallest p-value, linked to calcium ion binding in molecular function, and GO:0006986, significantly

associated with the response to unfolded proteins, displaying the largest enrichment factor. Notably, downregulated DEGs in the cellular component category prominently associated with mitochondria and peroxisomes (Fig. 6f, detailed in Table S2). Furthermore, Gene Set Enrichment Analysis (GSEA) was conducted on all detected genes. Significance was established when  $\text{FDR} < 0.25$ ,  $p < 0.05$ , and  $|\text{NES}| > 1$ . Genes located in the Mitochondrial matrix (GO:0005759) and Mitochondrial inner membrane (GO:0005743) were significantly downregulated in the CuCy + DSF group (Fig. 6g and h). Additionally, the DNA repair pathway showed significant inhibition in the same group (Fig. 6i). This suggests that damaged DNA incapable of normal repair, coupled with the release of pro-apoptotic substances from damaged mitochondria, contributes to cellular apoptosis.

### 3.7. Validation of the mitochondrial apoptotic pathway

The decline in mitochondrial membrane potential is a pivotal event during the early stages of apoptosis, wherein changes in the permeability of the outer mitochondrial membrane instigate cell death [52]. Mitochondrial membrane potential alteration is assessed using JC-1 dye, which forms aggregates emitting red fluorescence in the mitochondrial matrix when the membrane potential is high. Conversely, in damaged mitochondrial membranes, JC-1 exists as monomers emitting green fluorescence due to decreased aggregation in the matrix. This alteration in fluorescence colors signifies changes in mitochondrial membrane potential, indicating early cellular apoptosis. Notably, the combination drug group exhibited significantly more cells emitting green fluorescence compared to the control and single-drug groups, signifying apoptosis induction in the combination drug-treated cells (Fig. 7a).

DAPI is a fluorescent dye that binds to DNA, emitting a blue fluorescence upon excitation. The staining process allows for the examination of nuclear morphology alterations, a crucial aspect of apoptosis analysis. Throughout apoptosis, chromatin undergoes significant condensation, marginalization, and nuclear fragmentation [53]. These phenomena were notably observed in the combination drug treatment group (CuCy + DSF) in this study, while the control group and groups treated with individual drugs showcased numerous cells at different mitotic stages, such as metaphase and anaphase (Fig. 7b and c). Collectively, previous experimental outcomes suggest that the combination drug treatment induces apoptosis by instigating mitochondrial damage, consequently leading to anti-tumor effects. In the mitochondrial apoptotic pathway (Fig. 7d), mitochondrial damage leads to reduced membrane potential and integrity, resulting in the release of cytochrome c (Cyt c) into the cytoplasm. Cyt c forms an apoptosome with Apaf-1 and Caspase-9 [54], subsequently activating Caspase-9 [55]. Activated Caspase-9 cleaves Caspase-3 [56], initiating apoptosis through the activated Caspase-3-mediated cleavage effect [57]. Hence, the subsequent step is to corroborate the mitochondrial apoptotic pathway through molecular experiments. Cellular proteins from various treatment groups were collected, and Western blotting was performed to detect Caspase-9, Caspase-3, activated Caspase-9, and Caspase-3.

Following a 12-h drug treatment, there was no significant difference in Caspase-9 levels among the four groups. However, in the combination drug treatment group, the levels of Caspase-3, activated Caspase-9, and Caspase-3 were markedly higher compared to the control and individual drug treatment groups, signifying activation of the mitochondrial apoptotic pathway. Protein levels of Caspase-9, Caspase-3, Cleaved Caspase-9 exhibited no significant differences among the individual drug-treated groups and between these groups and the control. In the individual drug-treated groups (CuCy and DSF), the protein level of Cleaved Caspase-3 surpassed that in the control group. After 24 h of drug treatment, the levels of Caspase-9, Caspase-3, Cleaved Caspase-9 and Cleaved Caspase-3 in the combination drug treatment group were significantly higher than those in the control and individual drug treatment groups. Meanwhile, in the individual drug-treated groups (CuCy and DSF), the Caspase-9 protein level surpassed that in the

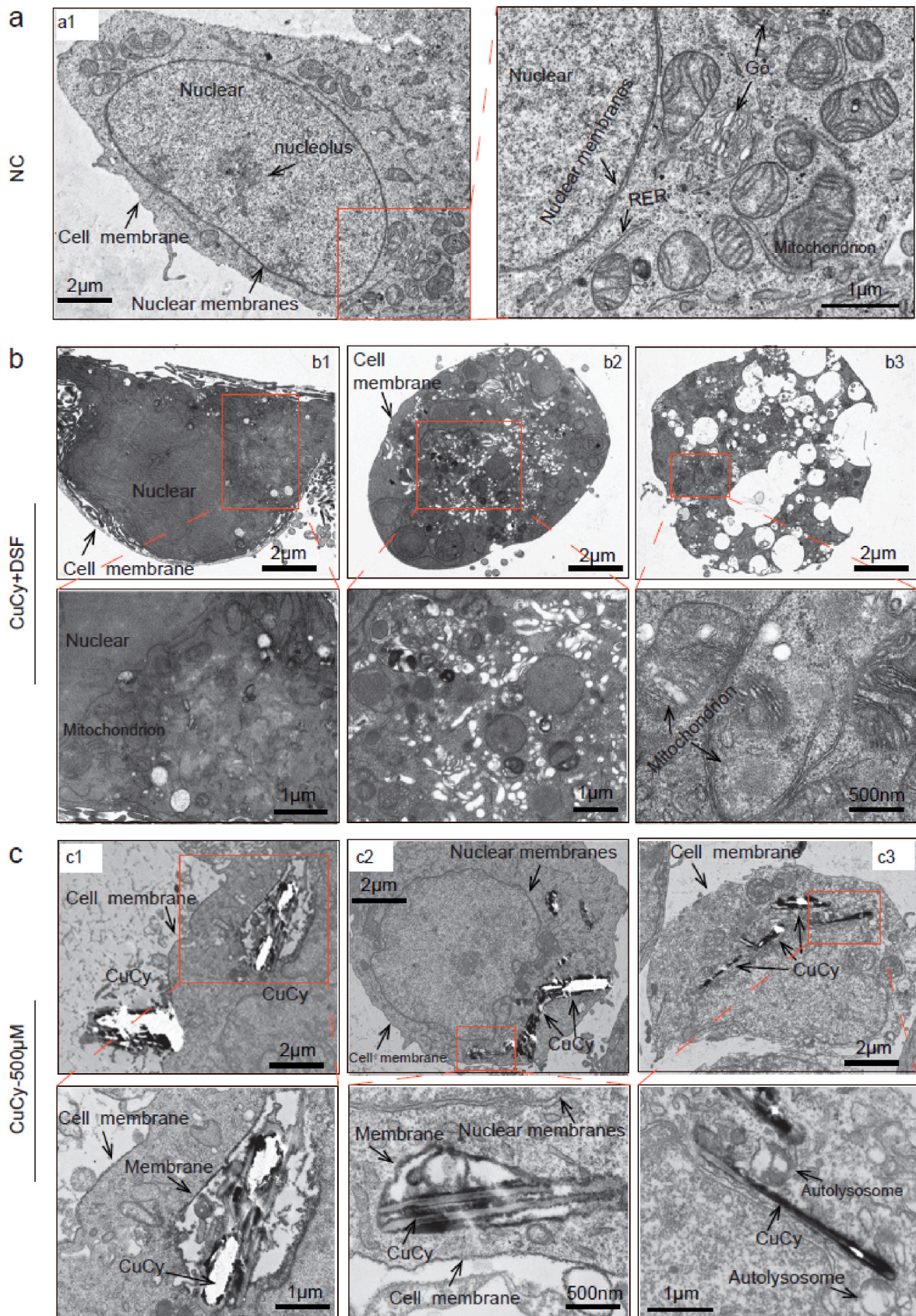


**Fig. 5.** TEM observations of Ishikawa cells after exposure to CuCy + DSF or CuCy alone. (a) Control group, (b) CuCy + DSF group (0.5 μM + 0.5 μM for 20 h), and (c) CuCy group (500 μM for 3 h).

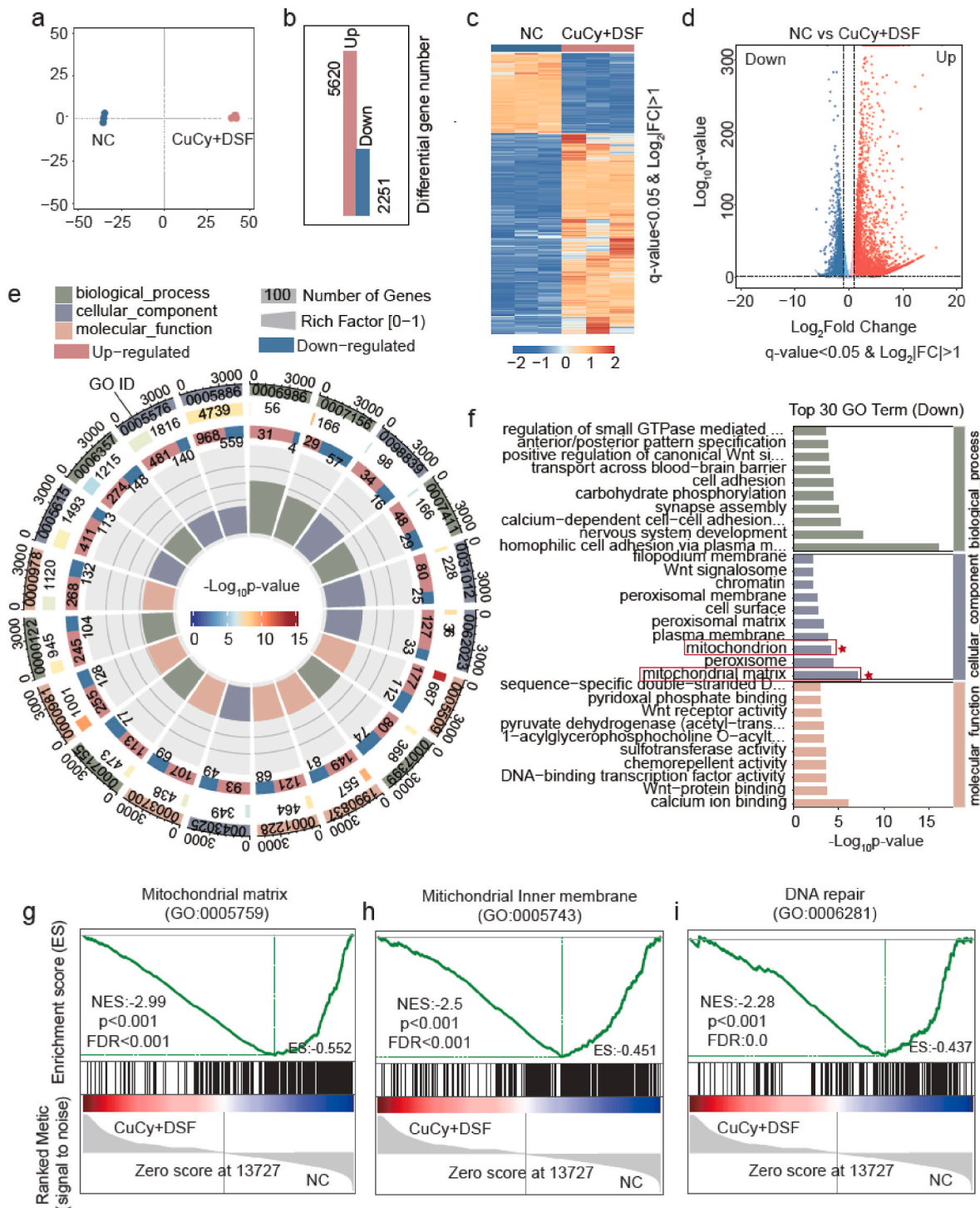


**Fig. 6.** RNA-seq analysis of Ishikawa cells after exposure to CuCy + DSF 12 h. (a) Principal Component Analysis (PCA) plot between NC and CuCy + DSF group; (b) Bar chart, (c) Cluster heatmap and (d) volcano plot of differentially expressed genes; (e) Circular plot of Gene Ontology (GO) enrichment analysis for all differentially expressed genes, showing the top 20 categories with the smallest p-values; (f) Bar chart of GO enrichment analysis for downregulated differentially expressed genes; (g–i) The Gene Set Enrichment Analysis (GSEA) of target GO terms.

control group, while Caspase-3, Cleaved Caspase-9 and Cleaved Caspase-3 levels showed no significant differences compared to the control (Fig. 7e–g).

In conclusion, the combined use of CuCy and DSF prompts apoptosis via mitochondrial damage, resulting in anti-tumor effects. Notably, the combination therapy exhibits superior efficacy compared to individual drug treatments.

### 3.8. Anti-tumor mechanism

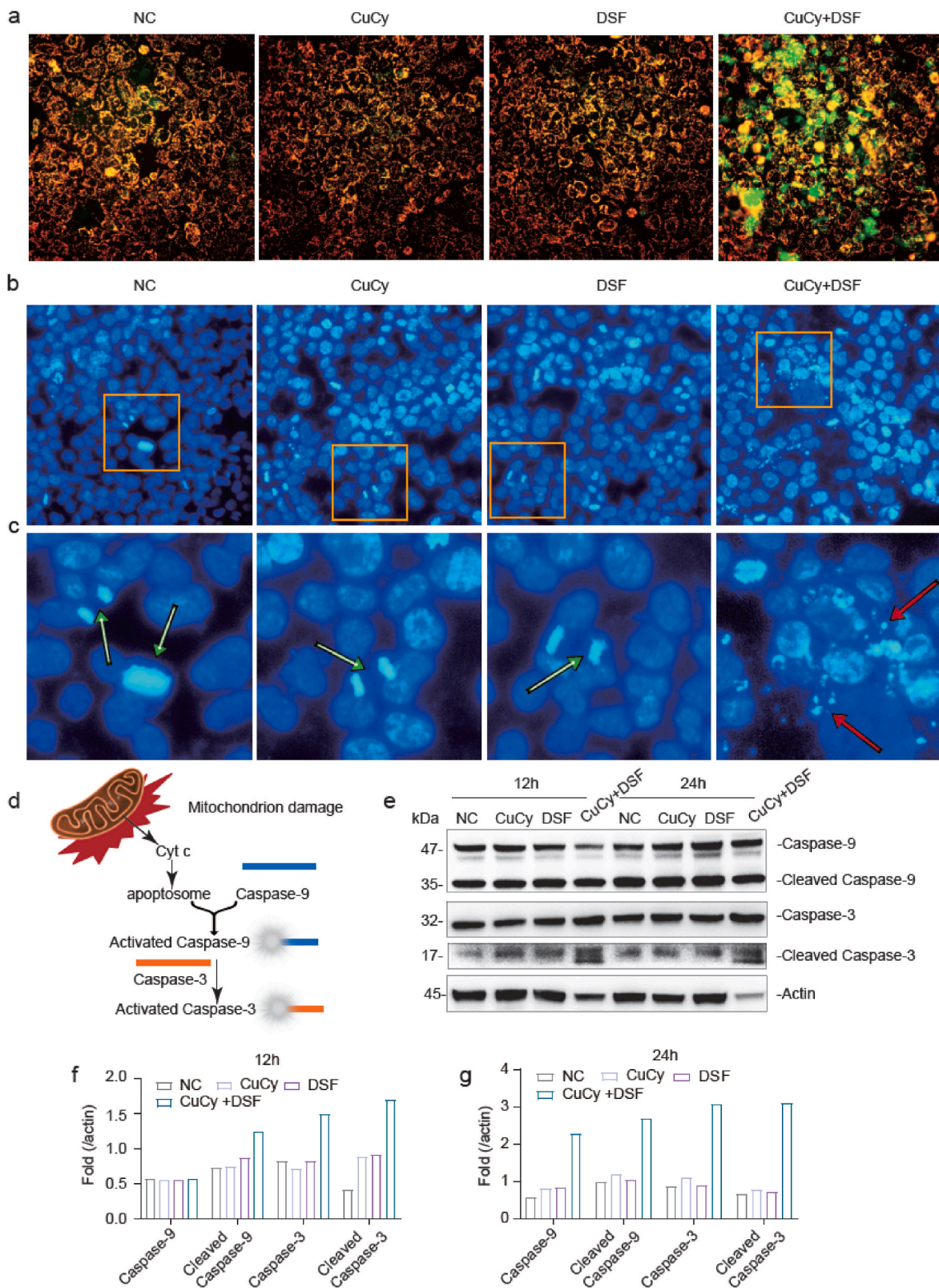


**Fig. 7.** Validation of the Mitochondrial Apoptotic Pathway. (a) Mitochondrial membrane potential assay and DAPI staining (b, c) after 12 h of treatment with CuCy and DSF alone or both in combination; (d) Schematic diagram of the mitochondrial apoptotic pathway; (e) Protein levels of Caspase-9, Caspase-3, Cleaved Caspase-9, and Cleaved Caspase-3 were evaluated by Western blotting after 12 and 24 h of drug treatment; (f, g) The pixel density analysis of the Western blotting results.

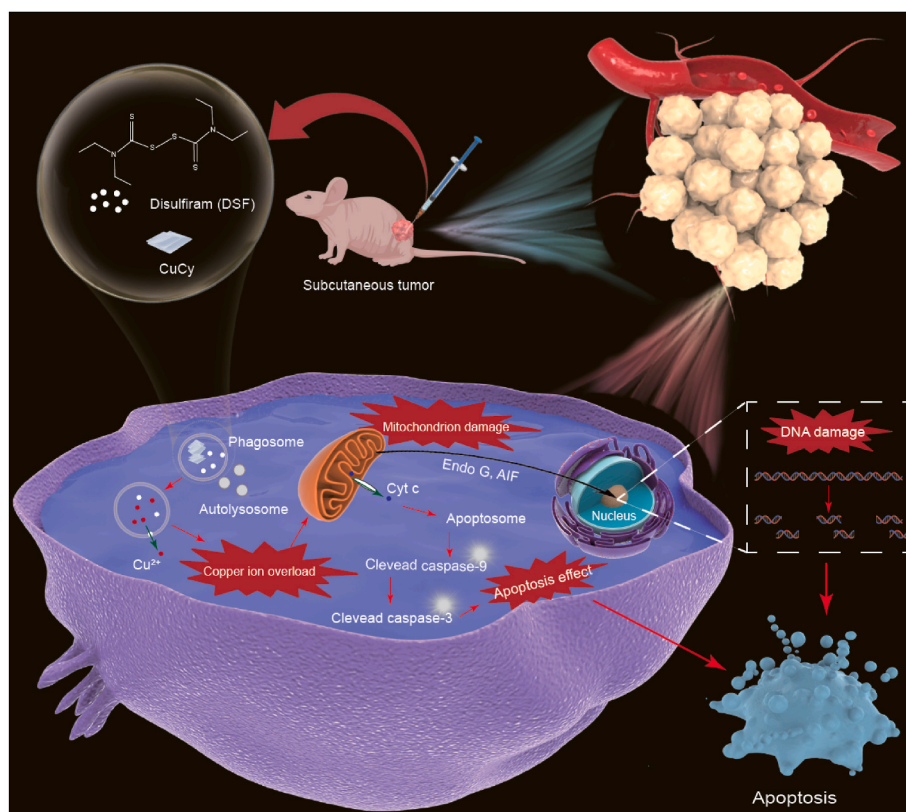


**Fig. 8.** Schematic diagram of the anti-tumor mechanism of the combination of CuCy and DSF. After successful subcutaneous tumorigenicity in nude mice, CuCy (0.5  $\mu\text{M}$ ) and DSF (0.5  $\mu\text{M}$ ) was mixed with saline and injected locally into the tumor tissue. Upon cellular uptake through phagocytosis, intracellular  $\text{Cu}^{2+}$  overload caused mitochondrial damage. This mitochondrial damage activates the mitochondrial apoptotic pathway, concomitantly releasing substances such as Endo G, which cleave DNA, ultimately triggering apoptosis and achieving anti-tumor effect.

## 4. Discussion

### 4.1. Anti-tumor mechanisms

The combined treatment of CuCy and DSF significantly hinders tumor growth and induces cell death both *in vitro* and *in vivo*, showcasing pronounced anti-tumor effects. Flow cytometry analysis unveiled cell death consistent with apoptosis (Fig. 3c), while DAPI staining exhibited apoptotic DNA characteristics (Fig. 7b). Strongly positive TUNEL signals were observed in the regional necrotic area of subcutaneous xenografts (Fig. 4l), and transmission electron microscopy confirmed apoptotic cell morphology (Fig. 5b). Detection of mitochondrial membrane potential revealed a decrease (Fig. 7a), suggesting mitochondrial impairment. Electron microscopy observations depicted mitochondrial alterations, including swelling, matrix lightning, dissolution, expansion, reduced cristae, and membrane rupture (Fig. 5b). Transcriptomic analysis at the molecular level revealed a substantial reduction in genes associated with mitochondria (Fig. 6f–h) and notable inhibition of mitochondrial translation pathways, signifying a link between apoptosis and mitochondria.

During the process of cellular apoptosis, mitochondria assume a pivotal role. Mitochondrial membrane rupture releases DNA-cutting effectors like Endo G and AIF, leading to DNA fragmentation. Transcriptomic analysis revealed significant inhibition of DNA repair pathways, complemented by DAPI staining showing nuclear fragmentation and condensation (Fig. 8b). Additionally, Cyt c, situated on the mitochondrial membrane, is released into the cytoplasm. Upon cytoplasmic release, it associates with Caspase-9, initiating a cascade reaction activating Caspase-9 and Caspase-3 (Fig. 7e), ultimately triggering apoptosis.

Transmission electron microscopy observations confirmed the

cellular uptake of materials through phagocytosis (Fig. 5c), with autophagic lysosomes observed near the materials (Fig. 5c). Consequently, the anti-tumor mechanism of the combined drug treatment is illustrated in Fig. 8. Upon co-treatment of tumor cells with CuCy and DSF at 0.5  $\mu\text{M}$  each, the drugs enter cells via phagocytosis. Under the influence of autophagic lysosomes, the material transforms into  $\text{Cu}^{2+}$ .  $\text{Cu}^{2+}$  ions enter the cytoplasm from the phagosome with the help of the copper ionophore DSF, inducing intracellular  $\text{Cu}^{2+}$  overload and ensuing mitochondrial damage. This mitochondrial damage triggers the mitochondrial apoptosis pathway, concomitantly releasing substances like Endo G to cleave DNA, culminating in apoptosis and achieving pronounced anti-tumor effects.

### 4.2. *In vivo* and *in vitro* anti-tumor effects

In both *in vitro* and *in vivo* experiments, extended exposure to DSF (0.5  $\mu\text{M}$ ) either as a standalone treatment or combined with CuCy (0.5  $\mu\text{M}$ ) significantly impeded the proliferation of Ishikawa cells (Figs. 3e and 4b, c, d) while inducing apoptosis in the cells (Figs. 3c and 4l). In the *in vitro* setting, within 24 h of treatment, the combination therapy group exhibited notably heightened anti-tumor effects compared to both monotherapy and control groups (Figs. 2d and 3b, c, d).

During *in vivo* experiments, both monotherapy and combination therapy effectively suppressed tumor growth. Notably, the combination of DSF and CuCy demonstrated a more pronounced inhibition of tumor growth compared to using CuCy alone, underscoring the enhanced anti-tumor efficacy of CuCy in conjunction with DSF. While the anti-tumor effect of DSF alone seemed marginally better than when combined with CuCy, no statistically significant difference was observed between the two groups ( $P > 0.5$ ). However, when DSF was administered alone, the mice exhibited a more rapid decrease in body weight compared to

the combination group, although this difference was not statistically significant ( $P > 0.5$ ). Moreover, two indicators of renal function were lower, suggesting a potential risk of malnutrition in the mice.

In contrast, the combination therapy group displayed a slower decline in body weight than the control group, with normal liver and kidney function indicators. This suggests a potential influence of CuCy on the distribution of DSF, potentially limiting its circulation, thereby mitigating its potential impact on the organism and enhancing the treatment's safety.

In conclusion, both *in vitro* and *in vivo* experiments demonstrated that combination therapy significantly inhibited tumor growth and promoted apoptosis. Notably, the *in vivo* combination therapy group exhibited reduced toxicity to the organism, suggesting a potential for enhanced safety compared to DSF administered alone.

#### 4.3. Clinical significance and future work

This study opted for local drug administration directly into the tumor tissue as opposed to intravenous or abdominal administration for several reasons. Firstly, the size of CuCy falls within the micrometer range, and administration via the tail vein or abdomen could potentially lead to localized settling of the material in other areas before reaching the tumor tissue. This settling might result in suboptimal anti-tumor effects due to lower drug concentrations within the tumor tissue and possible toxic effects in these settled regions.

Moreover, the uterus possesses its own distinctive cavity, which is semi-open. By loading drugs into an inert intrauterine device and placing it within the uterine cavity, local administration to the tumor tissue can be achieved while significantly reducing systemic circulation. This local administration approach minimizes drug consumption by the systemic circulation and decreases potential toxic effects on other bodily tissues. Notably, the drug doses of DSF and CuCy used in this study are among the lowest reported in relevant studies. For example, in a study of esophageal cancer, a significant anticancer effect was observed when DSF + CuCy was used *in vitro* at a dose of DSF (1  $\mu\text{M}$ ) + CuCy (4  $\mu\text{M}$ ) [30]. In a study of colorectal cancer, CuCy had a significant anticancer effect when used in combination with radiotherapy at a dose of 25 mg/l, i.e., 65.875  $\mu\text{M}$  [58]. The drugs, dosages and routes of administration in this study provide new options for the treatment of endometrial cancer when resistance, too many side effects or poor drug response occur with conventional drugs.

Future research will involve loading drugs onto intrauterine devices and examining drug release patterns and tumor-killing effects *in vitro*. This will include establishing an animal model of endometrial cancer, implanting drug-loaded intrauterine devices into the uterine cavity to study *in vivo* anti-tumor effects, and assessing the biocompatibility of materials with uterine tissue. Additionally, efforts will focus on creating organoid models using tissue samples from clinical endometrial cancer patients to explore the anti-tumor effects of drugs on endometrial cancer organoids. Lastly, metabolomics will be employed to identify potential drug targets.

Finally, we have to acknowledge some limitations of our study. Because of the species differences between mice and humans, the anti-tumor effects of drugs in clinical applications may not be as good as those observed in mouse experiments. However, we cannot avoid the problem of species differences, because we need to rely on animal experiments in the initial stage of drug research to make predictions and guide the subsequent experiments. In our future research, we will endeavor to establish human endometrial cancer organoids or patient-derived xenografts (PDX) to validate our findings, predict therapeutic responses, and provide guidance for precision medicine to fight against cancer.

## 5. Conclusions

In essence, this study unveils that the combined utilization of CuCy

and DSF triggers mitochondrial impairment and subsequent apoptosis in Ishikawa cells, culminating in potent anti-tumor outcomes. Initial observations through SEM unveiled the micrometer-scale sheet-like structure of CuCy material, while CCK8 experiments established the optimal drug concentrations for combined use at 0.5  $\mu\text{M}$ . Phenotypic studies conducted *in vitro* distinctly showcased the remarkable inhibition and disruption of angiogenesis alongside the induction of cell apoptosis upon their combined application. Moreover, *in vivo* investigations underscored a notable anti-tumor effect upon the combined administration of the drugs, attributing cell death to apoptosis. Intriguingly, when employed separately *in vivo*, both drugs exhibited significant inhibition of tumor growth. TEM findings suggested the cellular entry of CuCy via phagocytosis, and its combination with DSF induced mitochondrial swelling, membrane rupture, and overall mitochondrial damage, ultimately instigating cell apoptosis. Confirmation of mitochondrial damage and apoptotic effects was further substantiated through the mitochondrial membrane potential assay and DNA staining. Furthermore, transcriptomic analysis corroborated the substantial hindrance of both mitochondrial damage and DNA damage repair pathways in the combination treatment group. As a result, the amalgamation of CuCy and DSF emerges as a potent catalyst for inducing a robust anti-tumor effect.

#### Declaration of competing interest

The authors declare no conflict of interest.

#### Ethical agreement and compliance

The authors declare that they will follow the ethics for authorship, review and the authentic for the research and data.

#### CRediT authorship contribution statement

**Lijun Yang:** Writing – original draft, Visualization, Resources, Methodology, Investigation, Formal analysis, Conceptualization. **Cancan Yao:** Methodology, Investigation, Data curation. **Zhenning Su:** Methodology, Formal analysis, Data curation. **Yihao Fang:** Methodology, Data curation. **Nil Kanatha Pandey:** Methodology, Formal analysis, Data curation. **Eric Amador:** Investigation, Formal analysis, Data curation. **Tian Diao:** Methodology, Formal analysis, Data curation. **Guo Bao:** Project administration, Data curation, Conceptualization. **Derong Cao:** Supervision, Methodology, Conceptualization. **Xihua Chen:** Resources, Methodology, Investigation, Data curation. **Xiangbo Xu:** Methodology, Funding acquisition, Formal analysis. **Bin He:** Supervision, Project administration, Methodology, Funding acquisition, Formal analysis, Conceptualization. **Yufeng Zheng:** Writing – review & editing, Supervision, Project administration, Methodology, Investigation, Funding acquisition, Conceptualization. **Wei Chen:** Writing – review & editing, Validation, Supervision, Project administration, Funding acquisition, Conceptualization.

#### Acknowledgement

This work was supported by the National Natural Science Foundation of China (22071066), CAMS Innovation Fund for Medical Science (CIFMS, No. 2018-12M-1-004) and the project from department of Education, Jiangsu Province for the School of CHIPS at XJTU (EFP10120240023).

#### Appendix A. Supplementary data

Supplementary data to this article can be found online at <https://doi.org/10.1016/j.bioactmat.2024.02.009>.

## References

- [1] V. Makker, H. MacKay, I. Ray-Coquard, D.A. Levine, S.N. Westin, D. Aoki, A. Oaknin, Endometrial cancer, *Nat. Rev. Dis. Prim.* 7 (1) (2021) 88.
- [2] M.A. Sheikh, A.D. Althouse, K.E. Freese, S. Soisson, R.P. Edwards, S. Welburn, P. Sukumvanich, J. Comerci, J. Kelley, R.E. LaPorte, F. Linkov, USA endometrial cancer projections to 2030: should we be concerned? *Future Oncol.* 10 (16) (2014) 2561–2568.
- [3] S.J. Henley, E.M. Ward, S. Scott, J. Ma, R.N. Anderson, A.U. Firth, C.C. Thomas, F. Islami, H.K. Weir, D.R. Lewis, R.L. Sherman, M. Wu, V.B. Benard, L. C. Richardson, A. Jemal, K. Cronin, B.A. Kohler, Annual report to the nation on the status of cancer, part I: National cancer statistics, *Cancer* 126 (10) (2020) 2225–2249.
- [4] F. Amant, P. Moerman, P. Neven, D. Timmerman, E.v. Limbergen, I. Vergote, Endometrial cancer, *Lancet* 366 (2005) 491–505.
- [5] Z. Skrott, M. Mistrik, K.K. Andersen, S. Friis, D. Majera, J. Gursky, T. Ozdian, J. Bartkova, Z. Turi, P. Moudry, M. Kraus, M. Michalova, J. Vaclavkova, P. Dzubak, I. Vrobel, P. Pouckova, J. Sedlacek, A. Miklovicova, A. Kutt, J. Li, J. Mattova, C. Driessen, Q.P. Dou, J. Olsen, M. Hajdich, B. Cvek, R.J. Deshaies, J. Bartek, Alcohol-abuse drug disulfiram targets cancer via p97 segregase adaptor NPL4, *Nature* 552 (7684) (2017) 194–199.
- [6] K. Iljin, K. Ketola, P. Vainio, P. Halonen, P. Kohonen, V. Fey, R.C. Grafrström, M. Perälä, O. Kallioniemi, High-throughput cell-based screening of 4910 known drugs and drug-like small molecules identifies disulfiram as an inhibitor of prostate cancer cell growth, *Clin. Cancer Res.* 15 (19) (2009) 6070–6078.
- [7] B. Cvek, Nonprofit drugs as the salvation of the world's healthcare systems: the case of Antabuse (disulfiram), *Drug Discov. Today* 17 (9–10) (2012) 409–412.
- [8] J. Zha, F. Chen, H. Dong, P. Shi, Y. Yao, Y. Zhang, R. Li, S. Wang, P. Li, W. Wang, B. Xu, Disulfiram targeting lymphoid malignant cell lines via ROS-JNK activation as well as Nrf2 and NF- $\kappa$ B pathway inhibition, *J. Transl. Med.* 12 (2014) 163.
- [9] D. Chen, Q.C. Cui, H. Yang, Q.P. Dou, Disulfiram, a clinically used anti-alcoholism drug and copper-binding agent, induces apoptotic cell death in breast cancer cultures and xenografts via inhibition of the proteasome activity, *Cancer Res.* 66 (21) (2006) 10425–10433.
- [10] P. Dufour, J.M. Lang, C. Giron, B. Duclos, P. Haehnel, D. Jaeck, J.M. Jung, F. Oberling, Sodium dithiocarbamate as adjuvant immunotherapy for high risk breast cancer: a randomized study, *Biotherapy* 6 (1) (1993) 9–12.
- [11] R. Safi, E.R. Nelson, S.K. Chitneni, K.J. Franz, D.J. George, M.R. Zalutsky, D. P. McDonnell, Copper signaling axis as a target for prostate cancer therapeutics, *Cancer Res.* 74 (20) (2014) 5819–5831.
- [12] J.L. Allensworth, M.K. Evans, F. Bertucci, A.J. Aldrich, R.A. Festa, P. Finetti, N. T. Ueno, R. Safi, D.P. McDonnell, D.J. Thiele, S. Van Laere, G.R. Devi, Disulfiram (DSF) acts as a copper ionophore to induce copper-dependent oxidative stress and mediate anti-tumor efficacy in inflammatory breast cancer, *Mol. Oncol.* 9 (6) (2015) 1155–1168.
- [13] Y. Li, S.Y. Fu, L.H. Wang, F.Y. Wang, N.N. Wang, Q. Cao, Y.T. Wang, J.Y. Yang, C. F. Wu, Copper improves the anti-angiogenic activity of disulfiram through the EGFR/Src/VEGF pathway in gliomas, *Cancer Lett.* 369 (1) (2015) 86–96.
- [14] E.J. Ge, A.I. Bush, A. Casini, P.A. Cobine, J.R. Cross, G.M. DeNicola, Q.P. Dou, K. J. Franz, V.M. Gohil, S. Gupta, S.G. Kaler, S. Lutsenko, V. Mittal, M.J. Petris, R. Polishchuk, M. Ralle, M.L. Schilsky, N.K. Tonks, L.T. Vahdat, L. Van Aelst, D. Xi, P. Yuan, D.C. Brady, C.J. Chang, Connecting copper and cancer: from transition metal signalling to metalloplasia, *Nat. Rev. Cancer* 22 (2) (2022) 102–113.
- [15] P. Tsvetkov, S. Coy, B. Petrova, M. Dreishpoon, A. Verma, M. Abdusamad, J. Rossen, L. Joesch-Cohen, R. Humeidi, R.D. Spangler, J.K. Eaton, E. Frenkel, M. Kocak, S.M. Corsello, S. Lutsenko, N. Kanarek, S. Santagata, T.R. Golub, Copper induces cell death by targeting lipoylated TCA cycle proteins, *Science* 375 (6586) (2022) 1254–1261.
- [16] B. Shapiro, L. Eldjarin, The mechanism for the degradation of cystamine by ionizing radiation, *Radiat. Res.* 3 (4) (1955) 393–399.
- [17] J.G. Thoenes, R.G. Oshima, J.C. Crawhall, D.L. Olson, J.A. Schneider, Cystinosis. Intracellular cystine depletion by aminothiols in vitro and in vivo, *J. Clin. Invest.* 58 (1) (1976) 180–189.
- [18] D. Habibi, E. Ghaemi, D. Nematollahi, Synthesis of some novel silver-cysteamine complexes, *Molecules* 5 (12) (2000) 1194–1200.
- [19] B.A. Matrana, W.R. Bordelon, D.G. Davis, Polarography of copper (II)-(I) cysteine-cysteamine systems, *Anal. Lett.* 4 (7) (1971) 437–444.
- [20] L. Ma, W. Chen, G. Schatte, W. Wang, A.G. Joly, Y. Huang, R. Sammynaiken, M. Hossu, A new Cu–cysteamine complex: structure and optical properties, *J. Mater. Chem. C* 2 (21) (2014) 4239–4246.
- [21] N.K. Pandey, L. Chudal, J. Phan, L. Lin, O. Johnson, M. Xing, J.P. Liu, H. Li, X. Huang, Y. Shu, W. Chen, A facile method for the synthesis of copper-cysteamine nanoparticles and study of ROS production for cancer treatment, *J. Mater. Chem. B* 7 (42) (2019) 6630–6642.
- [22] Q. Zhang, X. Guo, Y. Cheng, L. Chudal, N.K. Pandey, J. Zhang, L. Ma, Q. Xi, G. Yang, Y. Chen, X. Ran, C. Wang, J. Zhao, Y. Li, L. Liu, Z. Yao, W. Chen, Y. Ran, R. Zhang, Use of copper-cysteamine nanoparticles to simultaneously enable radiotherapy, oxidative therapy and immunotherapy for melanoma treatment, *Signal Transduct. Targeted Ther.* 5 (1) (2020) 58.
- [23] S. Shrestha, J. Wu, B. Sah, A. Vanasse, L.N. Cooper, L. Ma, G. Li, H. Zheng, W. Chen, M.P. Antosh, X-ray induced photodynamic therapy with copper-cysteamine nanoparticles in mice tumors, *Proc. Natl. Acad. Sci. U. S. A.* 116 (34) (2019) 16823–16828.
- [24] B. Sah, J. Wu, A. Vanasse, N.K. Pandey, L. Chudal, Z. Huang, W. Song, H. Yu, L. Ma, W. Chen, M.P. Antosh, Effects of nanoparticle size and radiation energy on copper-cysteamine nanoparticles for X-ray induced photodynamic therapy, *Nanomaterials* 10 (6) (2020).
- [25] X. Chen, J. Liu, Y. Li, N.K. Pandey, T. Chen, L. Wang, E.H. Amador, W. Chen, F. Liu, E. Xiao, W. Chen, Study of copper-cysteamine based X-ray induced photodynamic therapy and its effects on cancer cell proliferation and migration in a clinical mimic setting, *Bioact. Mater.* 7 (2022) 504–514.
- [26] M. Yao, L. Ma, L. Li, J. Zhang, R. Lim, W. Chen, Y. Zhang, A new modality for cancer treatment—nanoparticle mediated microwave induced photodynamic therapy, *J. Biomed. Nanotechnol.* 12 (10) (2016) 1835–1851.
- [27] H. Zhou, Z. Liu, Z. Zhang, N.K. Pandey, E. Amador, W. Nguyen, L. Chudal, L. Xiong, W. Chen, Y. Wen, Copper-cysteamine nanoparticle-mediated microwave dynamic therapy improves cancer treatment with induction of ferroptosis, *Bioact. Mater.* 24 (2023) 322–330.
- [28] P. Wang, X. Wang, L. Ma, S. Sahi, L. Li, X. Wang, Q. Wang, Y. Chen, W. Chen, Q. Liu, Nanosensitization by using copper–cysteamine nanoparticles augmented sonodynamic cancer treatment, *Part. Part. Syst. Char.* 35 (4) (2018) 1700378.
- [29] W. Chen, Nanoparticle Based Therapeutics, *Index of Sciences*, 2023.
- [30] Y. Chang, F. Wu, N.K. Pandey, L. Chudal, M. Xing, X. Zhang, L. Nguyen, X. Liu, J. P. Liu, W. Chen, Z. Pan, Combination of disulfiram and copper-cysteamine nanoparticles for an enhanced antitumor effect on esophageal cancer, *ACS Appl. Bio Mater.* 3 (10) (2020) 7147–7157.
- [31] S. Chen, Y. Zhou, Y. Chen, J. Gu, fastp: an ultra-fast all-in-one FASTQ preprocessor, *Bioinformatics* 34 (17) (2018) i884–i890.
- [32] D. Kim, B. Langmead, S.L. Salzberg, HISAT: a fast spliced aligner with low memory requirements, *Nat. Methods* 12 (4) (2015) 357–360.
- [33] A. Roberts, C. Trapnell, J. Donaghey, J.L. Rinn, L. Pachter, Improving RNA-Seq expression estimates by correcting for fragment bias, *Genome Biol.* 12 (3) (2011) R22.
- [34] S. Anders, P.T. Pyl, W. Huber, HTSeq—a Python framework to work with high-throughput sequencing data, *Bioinformatics* 31 (2) (2015) 166–169.
- [35] M.I. Love, W. Huber, S. Anders, Moderated estimation of fold change and dispersion for RNA-seq data with DESeq2, *Genome Biol.* 15 (12) (2014) 550.
- [36] The gene Ontology Resource: 20 years and still Going strong, *Nucleic Acids Res.* 47 (D1) (2019) D330–d338.
- [37] A. Subramanian, P. Tamayo, V.K. Mootha, S. Mukherjee, B.L. Ebert, M.A. Gillette, A. Paulovich, S.L. Pomeroy, T.R. Golub, E.S. Lander, J.P. Mesirov, Gene set enrichment analysis: a knowledge-based approach for interpreting genome-wide expression profiles, *Proc. Natl. Acad. Sci. U. S. A.* 102 (43) (2005) 15545–15550.
- [38] V.K. Mootha, C.M. Lindgren, K.F. Eriksson, A. Subramanian, S. Sihag, J. Lehhar, P. Puigserver, E. Carlsson, M. Ridderstråle, E. Laurila, N. Houstis, M.J. Daly, N. Patterson, J.P. Mesirov, T.R. Golub, P. Tamayo, B. Spiegelman, E.S. Lander, J. N. Hirschhorn, D. Altshuler, L.C. Groop, PGC-1 $\alpha$ -responsive genes involved in oxidative phosphorylation are coordinately downregulated in human diabetes, *Nat. Genet.* 34 (3) (2003) 267–273.
- [39] J.D. Jiang, L. Denner, Y.H. Ling, J.N. Li, A. Davis, Y. Wang, Y. Li, J. Roboz, L. G. Wang, R. Perez-Soler, M. Marcelli, G. Bekesi, J.F. Holland, Double blockade of cell cycle at g(1)-s transition and m phase by 3-iodoacetamide benzoyl ethyl ester, a new type of tubulin ligand, *Cancer Res.* 62 (21) (2002) 6080–6088.
- [40] F. Niu, Y. Liu, Z. Jing, G. Han, L. Sun, L. Yan, L. Zhou, Y. Wu, Y. Xu, L. Hu, X. Zhao, Novel carbazole sulfonamide microtubule-stabilizing agents exert potent antitumor activity against esophageal squamous cell carcinoma, *Cancer Lett.* 420 (2018) 60–71.
- [41] Q. Fan, G. Bao, D. Ge, K. Wang, M. Sun, T. Liu, J. Liu, Z. Zhang, X. Xu, X. Xu, B. He, J. Rao, Y. Zheng, Effective easing of the side effects of copper intrauterine devices using ultra-fine-grained Cu-0.4Mg alloy, *Acta Biomater.* 128 (2022) 523–539.
- [42] K. Wang, G. Bao, Q. Fan, L. Zhu, L. Yang, T. Liu, Z. Zhang, G. Li, X. Chen, X. Xu, X. Xu, B. He, Y. Zheng, Feasibility evaluation of a Cu-38 Zn alloy for intrauterine devices: in vitro and in vivo studies, *Acta Biomater.* 138 (2022) 561–575.
- [43] D. Hanahan, R.A. Weinberg, The hallmarks of cancer, *Cell* 100 (1) (2000) 57–70.
- [44] D. Hanahan, R.A. Weinberg, Hallmarks of cancer: the next generation, *Cell* 144 (5) (2011) 646–674.
- [45] D. Hanahan, Hallmarks of cancer: new dimensions, *Cancer Discov.* 12 (1) (2022) 31–46.
- [46] N. Bouck, V. Stellmach, S.C. Hsu, How tumors become angiogenic, *Adv. Cancer Res.* 69 (1996) 135–174.
- [47] D. Hanahan, J. Folkman, Patterns and emerging mechanisms of the angiogenic switch during tumorigenesis, *Cell* 86 (3) (1996) 353–364.
- [48] E.G. Giannini, R. Testa, V. Savarino, Liver enzyme alteration: a guide for clinicians, *CMAJ (Can. Med. Assoc. J.)* 172 (3) (2005) 367–379.
- [49] H.Y. Lu, X.Y. Ning, Y.Q. Chen, S.J. Han, P. Chi, S.N. Zhu, Y. Yue, Predictive value of serum creatinine, blood urea nitrogen, uric acid, and  $\beta$ (2)-microglobulin in the evaluation of acute kidney injury after orthotopic liver transplantation, *Chin. Med. J.* 131 (9) (2018) 1059–1066.
- [50] Y. Gavrieli, Y. Sherman, S.A. Ben-Sasson, Identification of programmed cell death in situ via specific labeling of nuclear DNA fragmentation, *J. Cell Biol.* 119 (3) (1992) 493–501.
- [51] M. Barth, Y. Oulmi, H. Ehrenreich, L. Schilling, Pre-embedding immunogold labeling of TUNEL stain enables evaluation of DNA strand breaks and ultrastructural alterations in individual cells of neuronal tissue, *Acta Neuropathol.* 104 (6) (2002) 621–636.
- [52] F.J. Bock, S.W.G. Tait, Mitochondria as multifaceted regulators of cell death, *Nat. Rev. Mol. Cell Biol.* 21 (2) (2020) 85–100.
- [53] M. Rogalińska, Alterations in cell nuclei during apoptosis, *Cell. Mol. Biol. Lett.* 7 (4) (2002) 995–1018.

- [54] X. Jiang, X. Wang, Cytochrome c promotes caspase-9 activation by inducing nucleotide binding to Apaf-1, *J. Biol. Chem.* 275 (40) (2000) 31199–31203.
- [55] Q. Hu, D. Wu, W. Chen, Z. Yan, Y. Shi, Proteolytic processing of the caspase-9 zymogen is required for apoptosome-mediated activation of caspase-9, *J. Biol. Chem.* 288 (21) (2013) 15142–15147.
- [56] S.B. Bratton, G. Walker, S.M. Srinivasula, X.M. Sun, M. Butterworth, E.S. Alnemri, G.M. Cohen, Recruitment, activation and retention of caspases-9 and -3 by Apaf-1 apoptosome and associated XIAP complexes, *EMBO J.* 20 (5) (2001) 998–1009.
- [57] C. Pop, G.S. Salvesen, Human caspases: activation, specificity, and regulation, *J. Biol. Chem.* 284 (33) (2009) 21777–21781.
- [58] Z. Liu, L. Xiong, G. Ouyang, L. Ma, S. Sahi, K. Wang, L. Lin, H. Huang, X. Miao, W. Chen, Y. Wen, Investigation of copper cysteamine nanoparticles as a new type of radiosensitizers for colorectal carcinoma treatment, *Sci. Rep.* 7 (1) (2017) 9290.